

## Phase stabilities in the Pt-W system: Thermodynamic and electronic-structure calculations

A. Fernández Guillermet

*Consejo Nacional de Investigaciones Científicas y Técnicas, Centro Atómico Bariloche,  
8400 San Carlos de Bariloche, Argentina*

V. Ozoliņš, G. Grimvall, and M. Körling

*Department of Theoretical Physics, Royal Institute of Technology, S-100 44 Stockholm, Sweden  
(Received 27 October 1994)*

*Ab initio* electronic-structure calculations and the CALPHAD-type analysis of experimental phase diagrams and other thermodynamic information are known to give conflicting results for the enthalpy of several metastable transition metal phases, e.g., fcc W. We have simultaneously used *ab initio* total-energy calculations and the cluster expansion as well as CALPHAD methods in a study of the Pt-W phase diagram. The *ab initio* calculations show that fcc W is dynamically unstable for all long-wavelength shear modes at  $T = 0$  K. Even if fcc W becomes dynamically stable at high temperatures, the enthalpy of fcc W derived from CALPHAD analyses cannot be compared with the *ab initio* enthalpy of fcc W without a detailed knowledge of the vibrational entropy. Further, we show that the CALPHAD method can account for the phase diagram data and *ab initio* results for fcc and bcc Pt-W alloys provided that a metastable fcc W phase is given an unusually large entropy.

### I. INTRODUCTION

*Ab initio* electronic-structure calculations and the CALPHAD method<sup>1</sup> provide two main routes to the study of cohesive properties of metals and alloys. Both methods are now well established, and there are many attempts at a comparison between them.<sup>2-10</sup> Such work shows that, although there is often a good mutual agreement, there are also many examples of inconsistencies that have not yet been resolved. When the CALPHAD extrapolation methods have previously<sup>1,4-6,10,11</sup> been applied to W alloys, they yielded enthalpy differences  $\Delta H^{\text{fcc/bcc}}$  between the bcc and fcc pure W phases that are difficult to reconcile with  $\Delta H^{\text{fcc/bcc}}$  from *ab initio* calculations. Similar discrepancies are found also for some other transition metals, notably Os and Ru.<sup>2,6</sup> Recently, it has been noted that many of these systems showing discrepancies have metastable phases that are also dynamically unstable against shear.<sup>12-15</sup> Then, as argued by Craievich and Sanchez<sup>13</sup> and Craievich *et al.*,<sup>14</sup> one should not compare the energy difference calculated *ab initio* with the enthalpy difference ("lattice stability") derived in standard CALPHAD work. It is the purpose of this paper to further study the relation between *ab initio* electronic-structure calculations and CALPHAD work, with particular emphasis on the vibrational entropy, through a detailed study of the Pt-W system. There are several reasons why Pt-W is chosen for this work. The phase diagram of Pt-W is very simple (see below), with only fcc, bcc, and liquid phases present. The thermodynamics of pure bcc W is well understood.<sup>4,16</sup> The concentration range of the fcc phase field is the largest found for any binary W alloy, which makes Pt-W a good test case for the extrapolation

procedure in CALPHAD that predicts, e.g., the enthalpy  $H$  and the melting temperature  $T_f$  of fcc W.

Most previous comparisons of *ab initio* and CALPHAD predictions of phase stabilities assumed not only that the nonstable phase is dynamically stable, but also that its vibrational entropy is not very different from that of the stable phase. It may be expressed by the statement that the Debye temperatures are only weakly dependent on the crystal structure. On this assumption, it has been shown that *ab initio* and CALPHAD results for the enthalpy of fcc W cannot be reconciled.<sup>4</sup>

The *ab initio* calculations in the present paper not only confirm the instability of fcc W at 0 K under the tetragonal Bain distortion,<sup>13-15</sup> but show that fcc W is unstable for *all* long-wavelength shear modes. Since the vibrational entropy of dynamically unstable phases cannot be defined, there is a concentration range in the Pt-W system where also the Gibbs energy of the fcc phase is undefined, at least at low temperatures. The CALPHAD analysis should then be carried out without any *a priori* restrictions, e.g., on the variation of the Debye temperature. We perform such an analysis, in a critical discussion of the relation between quantities obtained in *ab initio* calculations and in the CALPHAD fit to the Pt-W phase diagram.

The outline of the paper is as follows. Our *ab initio* work in Sec. II first uses full-potential linear-muffin-tin-orbitals (FP-LMTO) total energy calculations and a cluster expansion (CE) method to obtain the enthalpy of mixing for fcc Pt-W alloys of all concentrations. Elastic constants and the frequencies of high-symmetry Brillouin-zone-boundary phonons in bcc and fcc W are obtained. The fcc W lattice is found to be dynamically unstable for long-wavelength shear, which indicates the

important role of the vibrational entropy as the W content is increased in the fcc Pt-W phase. In Sec. III we perform a thermodynamic CALPHAD-type analysis of the Pt-W phase diagram. A phase diagram is determined by the Gibbs energy  $G = H - TS$ , and this is the quantity the CALPHAD method extracts from the experimental data, while the *ab initio* electronic band-structure approach considers the enthalpy  $H$  and the entropy  $S$  as separate quantities. We therefore study in detail how  $H$  and  $S$  may covary in such a way that the good fit to the phase diagram is preserved. Our work shows how crucial it is to understand well the variation of  $S$  with the composition of the alloy. Section IV contains discussions and conclusions.

## II. ELECTRONIC-STRUCTURE CALCULATIONS AND CLUSTER EXPANSION

### A. Formalism of the cluster expansion

The cluster expansion<sup>17</sup> (CE) expresses any function of the atomic configuration in multicomponent systems in terms of series of independent cluster functions  $\Phi_\alpha$ . In the case of a binary alloy  $A_{1-c}B_c$ , spinlike variables  $\sigma_i$  are associated with each lattice site  $i$ . They take the values  $+1$  or  $-1$  depending on whether there is an atom  $A$  or  $B$  on the site. The cluster functions  $\Phi_\alpha$  are then defined as products of spin variables  $\sigma_{p_k}$  corresponding to the vertices of the cluster  $\alpha \equiv (p_1, \dots, p_n)$ , i.e.,

$$\Phi_\alpha(\sigma) \equiv \Phi_\alpha(\sigma_{p_1}, \dots, \sigma_{p_n}) = \sigma_{p_1} \cdots \sigma_{p_n}. \quad (1)$$

Clusters equivalent with respect to the space-group symmetry of the lattice are collected together in *orbits*. The orbits will be denoted by  $\alpha \equiv (n, q)$ , where  $n$  is the number of vertices and  $q$  enumerates the different orbits with the same  $n$ . If the number of equivalent clusters per lattice site is denoted by  $m_\alpha$ , then the configurational energy per lattice site can be expressed as

$$E(\sigma, V) = E_0(V) + \sum_{\alpha} m_{\alpha} E_{\alpha}(V) \bar{\Phi}_{\alpha}(\sigma), \quad (2)$$

where the summation is restricted to the different orbits,  $\bar{\Phi}_{\alpha}(\sigma)$  is the average of the cluster function over its orbit, and the empty-cluster term  $E_0(V)$  has been separated out. For the disordered alloy the orbit-averaged cluster functions all become  $\bar{\Phi}_{\alpha}(\sigma) = (1 - 2c)^{n_{\alpha}}$ , and the total energy is

$$E^{\text{dis}}(c, V) = E_0(V) + \sum_{n=1}^{\infty} \left[ \sum_q m_{(n,q)} E_{(n,q)}(V) \right] \times (1 - 2c)^n. \quad (3)$$

It was suggested by Connolly and Williams<sup>18</sup> that the effective cluster interactions (ECI's)  $E_{\alpha}$  in Eq. (2) can be obtained if the total energies of a set of periodic structures are known. Suppose that  $\{\phi\}$  is such a set of structures. Then the following sum of squares has to be minimized with respect to the unknown ECI's  $E_{\alpha}(V)$ :

$$w = \sum_{\{\phi\}} \omega_{\phi} \left[ E(\phi, V) - \sum_{\alpha} m_{\alpha} E_{\alpha}(V) \bar{\Phi}_{\alpha}(\sigma) \right]^2, \quad (4)$$

where  $\omega_{\phi}$  are suitable weighting factors.<sup>19</sup> We find that different possible choices of  $\omega_{\phi}$  marginally affect the extracted ECI's, and therefore we take  $\omega_{\phi} = 1$ .

Tables I and II give the data on the ordered Pt-W structures used to extract the ECI's for fcc and bcc Pt-W alloys. The *ab initio* calculated total energies are fitted to polynomial equations of state,

$$E(\phi, V) = E_0(\phi) + \frac{B(\phi)}{2V_0(\phi)} [V - V_0(\phi)]^2 - \frac{B(\phi)[1 + B'(\phi)]}{6V_0(\phi)^2} [V - V_0(\phi)]^3, \quad (5)$$

where  $\phi$  refers to different structures. The volume dependence of the ECI's is assumed to follow

TABLE I. Calculated enthalpies of formation  $\Delta^{\circ}H$ , equilibrium volumes  $V_0$ , bulk moduli  $B$ , and bulk derivatives  $B'$  of some of the face-centered-cubic Pt-W superstructures that were considered in the cluster expansion Eq. (4).

Composition	Strukturbericht	Pearson symbol	Space group	Prototype	$\Delta^{\circ}H$ (mRy/atom)	$V_0$ (a.u. <sup>3</sup> )	$B$ (Mbar)	$B'$
Pt	A1	cF4	$Fm\bar{3}m$	Cu	0.0	99.57	3.17	5.50
W	A1	cF4	$Fm\bar{3}m$	Cu	39.9	103.62	2.83	4.69
Pt <sub>3</sub> W	L1 <sub>2</sub>	cP4	$Pm\bar{3}m$	Cu <sub>3</sub> Au	-4.0	99.71	3.29	4.97
PtW <sub>3</sub>	L1 <sub>2</sub>	cP4	$Pm\bar{3}m$	Cu <sub>3</sub> Au	-0.8	100.50	3.25	4.37
PtW	L1 <sub>0</sub>	tP4	$P4/mmm$	CuAu	-11.8	99.50	3.35	4.25
Pt <sub>3</sub> W	D0 <sub>22</sub>	tI8	$I4/mmm$	TiAl <sub>3</sub>	-20.1	99.09	3.40	4.73
PtW <sub>3</sub>	D0 <sub>22</sub>	tI8	$I4/mmm$	TiAl <sub>3</sub>	4.19	101.01	3.20	4.46
PtW	"40"	tI8	$I4_1/amd$	NbP	-6.2	100.01	3.30	4.39
Pt <sub>2</sub> W	$\beta$ 1	tI6	$I4/mmm$		-20.4	98.96	3.35	4.50
PtW <sub>2</sub>	$\beta$ 2	tI6	$I4/mmm$		1.4	100.82	3.22	4.47
Pt <sub>2</sub> W	$\gamma$ 1	oI6	$Immm$	MoPt <sub>2</sub>	-27.3	98.74	3.43	4.55
PtW <sub>2</sub>	$\gamma$ 2	oI6	$Immm$	MoPt <sub>2</sub>	6.05	101.20	3.22	4.35
PtW	L1 <sub>1</sub>	hR32	$R\bar{3}m$	CuPt	-4.4	99.97	3.28	4.51
PtW	Z2	tP8	$P4/nmm$		-8.1	100.16	3.26	5.03

TABLE II. Calculated enthalpies of formation  $\Delta^0 H$ , equilibrium volumes  $V_0$ , bulk moduli  $B$ , and bulk pressure derivatives  $B'$  of body-centered-cubic Pt-W superstructures.

Compo- sition	Struktur- bericht	Pearson symbol	Space group	Proto- type	$\Delta^0 H$ (mRy/atom)	$V_0$ (a.u. <sup>3</sup> )	$B$ (Mbar)	$B'$
Pt	A2	<i>cI2</i>	<i>Im</i> $\bar{3}m$	W	7.0	100.64	2.98	4.93
W	A2	<i>cI2</i>	<i>Im</i> $\bar{3}m$	W	0.0	101.66	3.11	2.14
PtW	A <sub>1</sub>	<i>oC8</i>	<i>Cmmm</i>	$\gamma$ -IrV	7.1	101.07	3.15	3.89
Pt <sub>2</sub> W <sub>2</sub>	B11	<i>tP4</i>	<i>P4/nmm</i>	$\gamma$ -TiCu	6.8	102.04	3.08	4.06
PtW	B2	<i>cP2</i>	<i>Pm</i> $\bar{3}m$	CsCl	25.7	102.79	3.07	4.44
Pt <sub>2</sub> W <sub>2</sub>	B32	<i>cF16</i>	<i>Fd</i> $\bar{3}m$	NaTl	5.6	101.20	3.15	4.74
Pt <sub>2</sub> W	C11 <sub>b</sub>	<i>tI6</i>	<i>I4/mmm</i>	MoSi <sub>2</sub>	-1.6	101.22	3.19	4.55
PtW <sub>2</sub>	C11 <sub>b</sub>	<i>tI6</i>	<i>I4/mmm</i>	MoSi <sub>2</sub>	24.9	103.11	3.00	4.91
Pt <sub>3</sub> W	D0 <sub>3</sub>	<i>cF16</i>	<i>Fm</i> $\bar{3}m$	BiF <sub>3</sub> ,Cs <sub>3</sub> Sb	-0.3	101.04	3.16	4.60
PtW <sub>3</sub>	D0 <sub>3</sub>	<i>cF16</i>	<i>Fm</i> $\bar{3}m$	BiF <sub>3</sub> ,Cs <sub>3</sub> Sb	19.9	102.12	3.03	4.83
Pt <sub>3</sub> W	L6 <sub>0</sub>	<i>tP4</i>	<i>P4/mmm</i>	CuTi <sub>3</sub>	9.8	101.34	3.06	4.77
PtW <sub>3</sub>	L6 <sub>0</sub>	<i>tP4</i>	<i>P4/mmm</i>	CuTi <sub>3</sub>	14.7	101.99	3.05	4.73

$$E_\alpha(V) = E_\alpha^0 + E_\alpha^1(V - V_0) + E_\alpha^2(V - V_0)^2 + E_\alpha^3(V - V_0)^3, \quad (6)$$

where  $V_0$  is some suitable reference volume.

### B. Electronic structure and ECI's of Pt-W

The *ab initio* electronic-structure calculations have been performed using the local density approximation (LDA) and the full-potential linear-muffin-tin-orbitals (FP-LMTO) method as implemented by Methfessel.<sup>20</sup> The LMTO method employs a minimal basis set which consists of site-centered Hankel functions, augmented in a continuous and differentiable way by numerical solutions to the radial Schrödinger equation inside nonoverlapping muffin-tin spheres. Nonspherical and interstitial terms are calculated using the fitting procedures described in Ref. 20. We used the LDA exchange-correlation energy functional calculated by Ceperley and Alder<sup>21</sup> and parametrized by Vosko, Wilk, and Nusair.<sup>22</sup> The basis set contained *s*, *p*, *d*, and *f* orbitals from the LMTO envelope with the tail kinetic energy  $k = -0.01$  Ry and *s*, *p*, and *d* orbitals from the second LMTO envelope with  $k = -1.0$  Ry. Test calculations performed with larger basis sets showed that the total energies were converged to about 1 mRy/atom with respect to the size of the basis set. The core electrons were treated scalar relativistically and the core charge density was recalculated in each iteration. The nonspherical terms of the potential and charge density were expanded in spherical harmonics up to  $l_{\max} = 6$ . The number of **k** points was chosen so as to roughly correspond to 344 and 328 points in the irreducible parts of the Brillouin zones of simple fcc and bcc structures, respectively. To accelerate the convergence an artificial thermal broadening by 5 mRy of the electronic states near the Fermi level was used.

Uniform changes of volume are the only structural relaxations of periodic Pt-W structures studied in the present work. Changes in the total energies caused by deviations of *c/a* ratios and interatomic distances from their ideal values are not expected to affect considerably

the total energies of alloys if the constituents have rather small atomic size mismatch, which is the case in Pt-W. We have tested the effects of the *c/a* relaxation in the case of the fcc-based  $L1_0$  structure at a fixed lattice parameter  $a = 7.35$  a.u. The total energy was lowered by  $\delta E = 1.7$  mRy/atom when the *c/a* ratio changed from the ideal value  $\sqrt{2}$  to the equilibrium *c/a* = 1.52. In the tetragonal “40” and  $D0_{22}$  phases the corresponding changes were much smaller than in the  $L1_0$  phase. Since the objective of this work is the fcc-bcc enthalpy difference for W, i.e., a quantity  $\Delta H^{fcc/bcc} \approx 40$  mRy/atom, we neglect these relaxations.

Since the enthalpy curve for fcc Pt-W alloys is highly asymmetric around  $c = \frac{1}{2}$ , it was expected that many ECI's would have to be included in the CE [Eq. (2)] in order to reproduce it. Indeed, it was found that a very large set of periodic structures was needed to extract reliable values of the ECI's. The set of ECI's in Table III was selected after considering a hierarchy of fits to the *ab initio* equations of state from Table I. The total energies of ordered structures were reproduced with a root-mean-square error of 0.4 mRy/atom. The data given in Table III show that the absolute values of the ECI's generally decrease with the atomic volume, since the ordering energy vanishes in this limit. For fcc Pt-W alloys the ECI's corresponding to triplets and quadruplets are about as important as the pair ECI's. However, no important five-site ECI's were found, which suggested that the CE [Eq. (2)] could be truncated after the quadruplet terms. The large positive nearest-neighbor (NN) pair interaction suggests strong ordering tendencies, which are enhanced in the Pt-rich alloys by the substantial linear triplet ECI  $E_{(3,4)}$ . It is worth noting that the ECI  $E_{(3,4)}$  is considerably larger than that of the NN triangle  $E_{(3,1)}$ , which differs from results obtained in other systems<sup>23</sup> where  $E_{(3,1)}$  and  $E_{(3,4)}$  were approximately equal. Similarly, the ECI of the tetrahedron of nearest neighbors  $E_{(4,1)}$  is also smaller than those of the irregular tetrahedron  $E_{(4,2)}$  and the square of nearest neighbors  $E_{(4,3)}$ .

Figure 1 shows the enthalpies of formation of the disordered  $Pt_{1-c}W_c$  alloy and of the periodic structures considered in the present study. Several ordered struc-

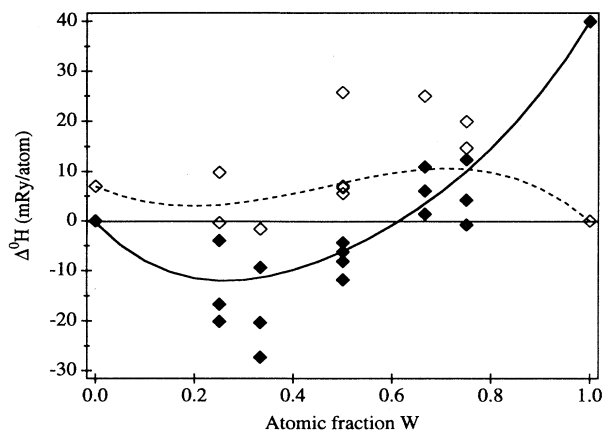


FIG. 1. The calculated *ab initio* enthalpies of formation of periodic fcc (filled diamonds) and bcc (empty diamonds) Pt-W superstructures. The continuous and dashed lines represent the enthalpies of formation of configurationally disordered fcc and bcc  $\text{Pt}_{1-c}\text{W}_c$  alloys.

tures are found to have lower enthalpies of formation than the configurationally disordered alloy, and therefore are likely to appear as the temperature decreases. The body-centered orthorhombic  $\gamma_1$  phase, which is actually observed in the Mo-Pt system, has a particularly low enthalpy of formation. This phase is not included in the recommended Pt-W phase diagram, and we predict that it should appear at low temperatures.

The ECI's given in Table III allow one to parametrize the configurational energetics of fcc Pt-W alloys. In

conjunction with some approximations for the configurational entropy, such as the cluster-variation method or Monte Carlo calculations, one could calculate the entire Pt-W phase diagram from first principles. However, we do not present such results here since we expect that the vibrational entropy  $S^{\text{vib}}$  plays a crucial role as the W-rich side of the phase diagram is approached (see Sec. IV), and it is still unfeasible to calculate  $S^{\text{vib}}$  for alloys from first principles. Further, the experimental phase diagram is well known only close to the melting temperatures and no ordered structures are established.

The results for the bcc-based Pt-W alloys are systematized in Tables II and IV and in Fig. 1. The NN pair interaction is strongly negative, causing a tendency towards phase separation. The convergence of the CE is rather fast, since already the quadruplet interactions are small. As in the case of fcc alloys, the linear triplet ECI  $E_{(3,3)}$  is very large and positive. From Fig. 1 we conclude that it is never energetically favorable to form disordered bcc  $\text{Pt}_{1-c}\text{W}_c$  at  $T = 0$  K. The existence of a narrow bcc phase field at high temperatures can be attributed to configurational entropy effects.

### C. Calculations of elastic constants and zone-boundary phonons

Recent *ab initio* studies<sup>13-15</sup> suggest that fcc W is mechanically unstable with respect to tetragonal distortions. Therefore we have performed extensive calculations of elastic constants and some zone-boundary phonon modes of fcc and bcc W. A cubic structure has three independent elastic moduli.<sup>24</sup> They can be

TABLE III. The effective cluster interactions for fcc-based Pt-W alloys, as defined in Eq. (6) with  $V_0 = 100$  a.u.<sup>2</sup>.

Symbol	Coordinates	Multiplicity $m_\alpha$	$E_\alpha^0$ (mRy)	$E_\alpha^1$ (mRy/a.u. <sup>3</sup> )	$E_\alpha^2$ (mRy/a.u. <sup>6</sup> )	$E_\alpha^3$ (mRy/a.u. <sup>9</sup> )
$E_{(0,1)}$		1	-6.1	-0.02	0.112	0.002
$E_{(1,1)}$	(000)	1	-22.7	0.44	-0.004	
$E_{(2,1)}$	(000), $(\frac{1}{2}0\frac{1}{2})$	6	2.1	-0.04		
$E_{(2,2)}$	(000), (100)	3	0.4			
$E_{(2,3)}$	(000), $(1\frac{1}{2}\frac{1}{2})$	24	0.0			
$E_{(2,4)}$	(000), (101)	6	1.1			
$E_{(2,5)}$	(000), $(\frac{3}{2}0\frac{1}{2})$	6	-0.1			
$E_{(3,1)}$	(000), $(\frac{1}{2}\frac{1}{2}0)$ , $(\frac{1}{2}0\frac{1}{2})$	8	0.2			
$E_{(3,2)}$	(000), $(\frac{1}{2}0\frac{1}{2})$ , (100)	12	0.05			
$E_{(3,3)}$	(000), $(\frac{1}{2}0\frac{1}{2})$ , $(1\frac{1}{2}\frac{1}{2})$	24	-0.4			
$E_{(3,4)}$	(000), $(\frac{1}{2}0\frac{1}{2})$ , (101)	6	1.6	-0.62		
$E_{(4,1)}$	(000), $(\frac{1}{2}0\frac{1}{2})$ , $(\frac{1}{2}\frac{1}{2}0)$ , $(0\frac{1}{2}\frac{1}{2})$	2	-0.4	0.01		
$E_{(4,2)}$	(000), $(\frac{1}{2}0\frac{1}{2})$ , $(\frac{1}{2}\frac{1}{2}0)$ , (100)	12	1.1	-0.01		
$E_{(4,3)}$	$(\frac{1}{2}0\frac{1}{2})$ , $(0\frac{1}{2}\frac{1}{2})$ , $(\frac{1}{2}1\frac{1}{2})$ , $(1\frac{1}{2}\frac{1}{2})$	3	-1.5	0.02		

TABLE IV. The effective cluster interactions for bcc-based Pt-W alloys, as defined in Eq. (6) with  $V_0 = 101.5$  a.u.<sup>3</sup>.

Symbol	Coordinates	Multiplicity $m_\alpha$	$E_\alpha^0$ (mRy)	$E_\alpha^1$ (mRy/a.u. <sup>3</sup> )	$E_\alpha^2$ (mRy/a.u. <sup>6</sup> )	$E_\alpha^3$ (mRy/a.u. <sup>9</sup> )
$E_{(0,1)}$		1	7.7	0.01	0.104	0.002
$E_{(1,1)}$	(000)	1	-10.84	0.22	0.003	
$E_{(2,1)}$	(000), ( $\frac{1}{2}\frac{1}{2}\frac{1}{2}$ )	4	-2.0	0.03	0.001	
$E_{(2,2)}$	(000), (100)	3	1.1	-0.05		
$E_{(2,3)}$	(000), (101)	6	0.4			
$E_{(2,4)}$	(000), ( $\frac{3}{2}\frac{1}{2}\frac{1}{2}$ )	12	-0.25			
$E_{(2,5)}$	(000), (111)	4	0.6	0.01		
$E_{(3,1)}$	(000), ( $\frac{1}{2}\frac{1}{2}\frac{1}{2}$ ), (100)	12	0.3			
$E_{(3,2)}$	(000), ( $\frac{1}{2}\frac{1}{2}\frac{1}{2}$ ), (101)	12	0.2			
$E_{(3,3)}$	(000), ( $\frac{1}{2}\frac{1}{2}\frac{1}{2}$ ), (111)	4	2.0	-0.02		
$E_{(4,1)}$	(000), ( $\frac{1}{2}\frac{1}{2}\frac{1}{2}$ ), ( $\frac{1}{2}\frac{1}{2}\frac{-1}{2}$ ), (100)	6				
$E_{(4,2)}$	(000), ( $\frac{1}{2}\frac{1}{2}\frac{1}{2}$ ), ( $\frac{1}{2}\frac{1}{2}\frac{-1}{2}$ ), (110)	6	-0.2			

obtained from the curvatures of the total energy as a function of the lattice distortions described below. The bulk modulus  $B = \frac{1}{3}(C_{11} + 2C_{12})$  gives the second-order changes in the total energy upon uniform compression,  $B = V \left( \frac{\partial^2 E}{\partial V^2} \right)$ . The tetragonal shear constant  $C' = \frac{1}{2}(C_{11} - C_{12})$  is calculated as<sup>25</sup>

$$C' = \frac{2}{3} \lim_{\gamma \rightarrow 0} \delta_\gamma E / \gamma^2, \quad (7)$$

where  $\delta_\gamma E$  is the strain energy induced by the following shear:

$$\begin{pmatrix} e^{-\gamma/2} & 0 & 0 \\ 0 & e^{-\gamma/2} & 0 \\ 0 & 0 & e^\gamma \end{pmatrix}. \quad (8)$$

The third independent elastic constant  $C_{44}$  can be calculated from

$$C_{44} = \frac{1}{2} \lim_{\gamma \rightarrow 0} \delta_\gamma E / \gamma^2, \quad (9)$$

if the applied monoclinic shear is given by

$$\begin{pmatrix} 1 & \gamma & 0 \\ \gamma & 1 & 0 \\ 0 & 0 & \frac{1}{1-\gamma^2} \end{pmatrix}. \quad (10)$$

Zone-boundary phonon frequencies were obtained using the “frozen-phonon” method.<sup>26,27</sup> The total energies of frozen-in phonon configurations of the lattice are calculated and the phonon frequencies are obtained from the resultant energy-displacement curves. Since the energy differences involved are of the order of 1 mRy/atom, a relative accuracy of approximately 0.01 mRy/atom is usually required. Although the strain energies are not ex-

tremely sensitive to the size of the LMTO basis set, the accuracy of the  $\mathbf{k}$ -point summations is very important.<sup>27</sup> Our calculations used  $\mathbf{k}$  meshes with 256 points in the irreducible parts of the Brillouin zones of bcc and fcc lattices, while a Gaussian smearing of 5 mRy was applied to each electronic state. We chose the  $\mathbf{k}$  meshes of the distorted lattices such that in the case of zero distortion the undistorted  $\mathbf{k}$  mesh of cubic symmetry was recovered.

Table V summarizes the results. The calculated phonon frequencies and elastic constants of bcc W are within 80% of the experimental data. For fcc W our calculations confirm that the elastic constant  $C'$  of fcc W is negative,<sup>13-15</sup> which implies a dynamical instability

TABLE V. The calculated elastic constants and longitudinal ( $L$ ) and transverse ( $T_1, T_2$ ) phonon frequencies at zone-boundary points  $H$ ,  $N$ ,  $X$ , and  $L$  in fcc and bcc W at  $V = 103.37$  a.u.<sup>3</sup>.

		Theor.	Expt.	
bcc W	Elastic constants (Mbar)			
	$C' = \frac{1}{2}(C_{11} - C_{12})$	1.78	1.638	
	$C_{44}$	1.55	1.631	
	Phonon frequencies (THz)			
	$L(H)$	5.38	5.5	
	$L(N)$	6.88	6.75	
	$T_1(N)$	4.73	4.40	
	$T_2(N)$	4.09	4.15	
	fcc W	Elastic constants (Mbar)		
		$C' = \frac{1}{2}(C_{11} - C_{12})$	-2.32	
$C_{44}$		-2.56		
Phonon frequencies (THz)				
$L(X)$		6.65		
$T(X)$		2.82		
$T(L)$		1.04		

with respect to tetragonal distortions. Furthermore, we find that the  $C_{44}$  elastic constant of fcc W is also negative, which causes *all* long-wavelength transverse phonon frequencies to be imaginary. Therefore *fcc W is dynamically unstable with respect to all lattice deformations corresponding to acoustic shear modes*. However, it is seen from Table V that zone-boundary phonon frequencies of fcc W are real and of the same magnitude as in bcc W, except for the soft  $T(L)$  mode with a substantially anharmonic character. This behavior implies a strong and unusual wave-vector dependence of  $\omega_{\mathbf{q}\lambda}^2$ , being negative only in part of the Brillouin zone, close to  $\mathbf{q} = \mathbf{0}$ . We suggest that this explains why a previous first-principles study of the vibrational properties of transition metals<sup>28</sup> did not find anomalies in the second moment  $\langle \omega^2 \rangle$  of the frequency spectra of fcc W. Consequences of negative  $C'$  and  $C_{44}$  for the vibrational entropy,  $S_{\text{vib}} \sim \langle \ln \omega \rangle$ , will be discussed in more detail in Sec. IV.

### III. THERMODYNAMIC ANALYSIS

#### A. Definitions and models

The Gibbs energy per mole of atoms,  $G_m^\phi$ , of the phase  $\phi$  (with  $\phi = \text{bcc, fcc, or liquid}$ ) of the Pt-W system at high temperatures was described by a substitutional solution model,

$$G_m^\phi = x_{\text{Pt}} {}^0G_{\text{Pt}}^\phi + x_{\text{W}} {}^0G_{\text{W}}^\phi + RT(x_{\text{Pt}} \ln x_{\text{Pt}} + x_{\text{W}} \ln x_{\text{W}}) + {}^E G_m^\phi. \quad (11)$$

$R$  is the gas constant,  $T$  the temperature,  $x_i$  is the atomic fraction of the element  $i$  ( $i = \text{Pt, W}$ ), and  ${}^0G_i^\phi$  is the Gibbs energy of the pure element  $i$  in the structure  $\phi$ . The  ${}^0G_i^\phi$  values were referred to the enthalpies  ${}^0H_i^{\text{st}}$  of the stable (st) forms of the elements  $i$  at  $T_0 = 298.15$  K and  $P_0 = 1$  bar. The functions  ${}^0G_i^\phi(T) - {}^0H_i^{\text{st}}$  for the stable phases of W ( $\phi = \text{bcc or liquid}$ ) and Pt ( $\phi = \text{fcc or liquid}$ ) were taken from Refs. 11 and 29. The remaining parameters,  ${}^0G_{\text{Pt}}^{\text{bcc}}$  and  ${}^0G_{\text{W}}^{\text{fcc}}$ , describe the nonstable modifications of W and Pt. They were related to the stable forms as

$${}^0G_{\text{W}}^{\text{fcc}} - {}^0G_{\text{W}}^{\text{bcc}} = A_{\text{W}} - B_{\text{W}}T, \quad (12)$$

$${}^0G_{\text{Pt}}^{\text{bcc}} - {}^0G_{\text{Pt}}^{\text{fcc}} = A_{\text{Pt}} - B_{\text{Pt}}T. \quad (13)$$

The linear expressions on the right sides of Eqs. (12) and (13) will be referred to as “lattice stabilities,” in accordance with the CALPHAD convention. The constants  $A_i$  and  $B_i$  represent enthalpy and entropy differences between the nonstable and the stable forms of the elements  $i$ . They are discussed below. The last term in Eq. (11) is the excess Gibbs energy  ${}^E G_m^\phi$  which accounts phenomenologically for the nonideal behavior of the phase  $\phi$ . It was treated in the subregular-solution approximation of the Redlich-Kister<sup>30</sup> power series,

$${}^E G_m^\phi = x_{\text{Pt}} x_{\text{W}} [{}^0L^\phi + {}^1L^\phi(x_{\text{Pt}} - x_{\text{W}})]. \quad (14)$$

The composition-independent parameters  ${}^0L^\phi$  and  ${}^1L^\phi$

account for the interaction between atoms of Pt and W in the phase  $\phi$ . They were assumed to be independent of temperature. This approximation makes  $G_m^\phi$  identical to the enthalpy of formation of the phase from the elements with the structure  $\phi$  at all temperatures.

#### B. Enthalpy of formation of fcc W at 0 K

It has previously been suggested<sup>4,6,31</sup> that the discrepancy between *ab initio* and CALPHAD values for the structural enthalpy difference for the stable and nonstable modifications of an element might be due to the use of low-order polynomials in the concentration variable, when the excess functions of the solution phases are described. This point has not previously been adequately discussed and we therefore consider in some detail various fitting procedures that can be used. Lacking direct measurements of the heat of formation for fcc Pt-W, we shall rely on the enthalpy of formation data obtained from the cluster expansion as described below. Using the models in Sec. III A we write the enthalpy of formation of the fcc Pt-W alloy from fcc Pt and bcc W at 0 K as

$$\begin{aligned} \Delta H_m^{\text{fcc}} &= H_m^{\text{fcc}} - x_{\text{W}} {}^0H_{\text{W}}^{\text{bcc}} - x_{\text{Pt}} {}^0H_{\text{Pt}}^{\text{fcc}} \\ &= x_{\text{W}} A_{\text{W}} + x_{\text{Pt}} x_{\text{W}} [{}^0L^\phi + {}^1L^\phi(x_{\text{Pt}} - x_{\text{W}})]. \end{aligned} \quad (15)$$

Equation (15) was fitted to the data obtained from the *ab initio* cluster expansion of the heat of formation. Figure 2(a) shows that our  $\Delta H_m^{\text{fcc}}$  (solid line) agrees well with the input CE values (filled triangles). In particular, our fit gives  $A_{\text{W}} = 38.5$  mRy/atom, to be compared with our *ab initio* calculated structural energy difference 40 mRy/atom. In order to test how sensitive this result is to the extent of the composition range covered by the input enthalpy values, we repeated the fit when

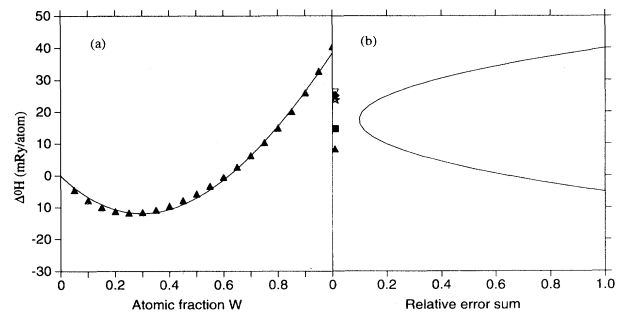


FIG. 2. (a) The enthalpy of formation of the fcc Pt-W phase ( $\Delta H_m^{\text{fcc}}$ ) obtained from the *ab initio* cluster expansion (CE) calculations (filled triangles). The solid line represents a subregular-solution fit [Eq. (15)] to the CE enthalpy values. (b)  $A_{\text{W}}$  versus the error sums in a series of fits to CE enthalpies of formation. The symbols refer to thermodynamic estimates of the structural enthalpy difference  $\Delta {}^0H_{\text{W}}^{\text{fcc/bcc}}$  by Kaufman and Bernstein (Ref. 1, filled triangle), Gustafson (Ref. 11, filled square), Saunders, Miodownik, and Dinsdale (Ref. 5, filled diamond), and the upper bounds to  $\Delta {}^0H_{\text{W}}^{\text{fcc/bcc}}$  according to Grimvall, Thiessen, and Fernández Guillermet (Ref. 4, star) and Fernández Guillermet and Hillert (Ref. 6, empty triangle).

including  $\Delta H_m^{\text{fcc}}$  values only up to  $x_W = 0.75$ . The fitted  $\Delta H_m^{\text{fcc}}$  reproduces better the input information, but the enthalpy difference for fcc W, 26 mRy/atom, is significantly lower than the theoretical value. The reason is that the fitted function of Eq. (15) has an inflection point at  $x_W = 1/2 + (1/6)({}^0L/{}^1L)$ , which for certain  ${}^0L$  and  ${}^1L$  yields a decrease in the slope of  $\Delta H_m^{\text{fcc}}$  vs  $x_W$  before reaching  $x_W = 1$ . The risk for such a behavior increases when  ${}^0L$  and  ${}^1L$  are determined from a limited composition range and one cannot monitor the fit at large W contents. We conclude that a Redlich-Kister low-order polynomial can represent well the *ab initio* results for the heats of formation (see Fig. 2), but without additional information in the range of  $x_W$  not covered by experiments, the extrapolation to pure fcc W would depend critically on the amount of information included in the fit. As a consequence, the CALPHAD method does not usually adopt such an extrapolation to estimate  $A_W$ .

An alternative procedure<sup>31–33</sup> is to vary systematically  $A_W$  in a series of fits of Eq. (15) to the experimental data in the region where fcc is a stable phase, and display  $A_W$  as a function of the error sum. When the error sum has its minimum, one recovers  $A_W$  from the first type of fit above. However, the alternative method gives more insight since it allows one to judge what is the range of  $A_W$  values that would lead to an acceptable fit. This procedure was tested by performing systematic fits to the *ab initio* CE values for the enthalpy of formation at 0 K, covering the range  $0 \leq x_W \leq 0.65$ . The error sum (in arbitrary units) is plotted versus the assumed  $A_W$  value in Fig. 2(b). It is evident that the best fit to this set of  $\Delta H_m^{\text{fcc}}$  values is obtained when  $A_W$  is about 18 mRy/atom. This value agrees with the most recent fcc-bcc enthalpy differences for W obtained in CALPHAD-type analyses.<sup>5,11</sup>

### C. Analysis of the Pt-W phase diagram

The Pt-W phase diagram has been determined only above 2000 K,<sup>34–39</sup> which comprises fcc + liquid, fcc + bcc, and bcc + liquid two-phase equilibria. The fcc + bcc + liquid three-phase equilibrium at 2733 K is also well established.<sup>37–39</sup> At about 1673 K some intermediate phases have been detected,<sup>39</sup> and it is accepted that they do not form from the liquid.<sup>39</sup> Since the information available is not enough to establish their equilibrium boundaries or thermodynamic properties, they were excluded from the present analysis. Experimental information on the fcc + liquid, fcc + bcc, bcc + liquid, and fcc + bcc + liquid equilibria was analyzed using Eq. (11) for the Gibbs energy of each solution phase and Eqs. (12) and (13) for the nonstable forms of W and Pt.

Since our main concern in this paper is the structural enthalpy difference for W, we fixed the properties of Pt as follows.  $A_{\text{Pt}} = 7.02$  mRy/atom was taken from our *ab initio* calculations. Lacking theoretical or experimental information to determine  $B_{\text{Pt}}$ , which is related to the entropy of bcc Pt, we adopted a somewhat larger entropy in the fcc phase and assumed  $B_{\text{Pt}} = -0.2R$ .<sup>6,32</sup> The bcc phase is stable in a very small composition range, close

to pure W. Since the information available is not enough to determine both interaction parameters we let  ${}^0L^{\text{bcc}} = -{}^1L^{\text{bcc}}$ . Then the excess Gibbs energy  ${}^E G_m^{\text{bcc}}$  [Eq. (14)] vanishes when  $x_{\text{Pt}} \rightarrow 1$ . This ensures that the bcc phase will not become stable when approaching pure Pt, where the structural enthalpy difference between bcc and fcc is relatively small (see above).

Equation (11) was used to describe the liquid phase, with both  ${}^0L^{\text{liq}}$  and  ${}^1L^{\text{liq}}$  treated as free parameters. It remains to discuss the fcc phase.  ${}^0L^{\text{fcc}}$  and  ${}^1L^{\text{fcc}}$  and the lattice stability of fcc W described by Eq. (12) were free parameters, determined by the best fit to the phase diagram. Since the temperature range covered by the experimental information is rather small, we could not let both  $A_W$  and  $B_W$  in Eq. (12) vary freely. Instead  $A_W$  was varied systematically in a series of fits where  $B_W$  and the interaction parameters for the fcc, bcc, and liquid phases were determined by minimizing the sum of the squares of the differences between experimental and calculated values of the equilibrium boundaries. In

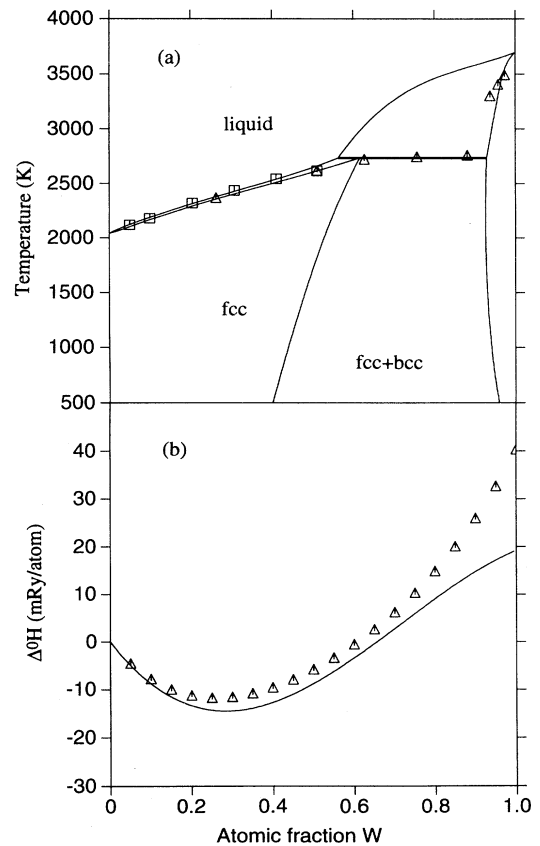


FIG. 3. (a) The Pt-W phase diagram calculated in the subregular-solution approximation and with the fcc W lattice stabilities given by  $A_W = 19.2$  mRy/atom and  $B_W = 0.8R$ . Symbols denote experimental data according to Ref. 34 (squares) and Ref. 36 (triangles). (b) The enthalpy of formation  $\Delta H_m^{\text{fcc}}$  of the fcc phase in the Pt-W system, versus composition. The solid line represents values calculated from the thermodynamic description. Triangles represent the enthalpies of formation from *ab initio* CE calculations.

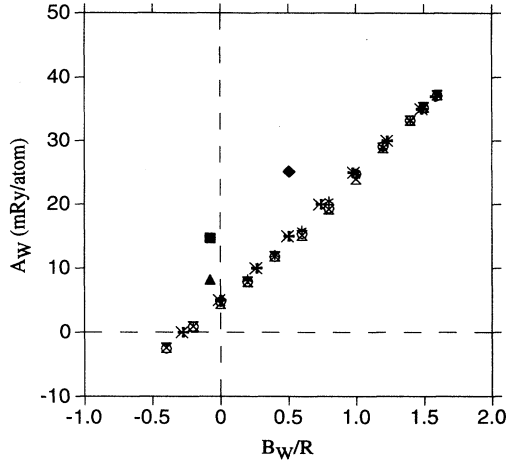


FIG. 4. The structural enthalpy difference  $A_W$  between fcc and bcc W, versus the corresponding entropy difference  $B_W$  at high temperatures, obtained from systematic fits to the Pt-W phase diagram. The three filled symbols refer to thermodynamic estimates, as in Fig. 2.

a second series of fits,  $B_W$  was varied systematically and  $A_W$  was determined in the optimization.

In Fig. 3(a) we compare the calculated (solid line) and the experimental phase diagram data (symbols) for the optimum parameters when  $B_W = 0.8R$ . This fit gives  $A_W = 19.2$  mRy/atom, which is about half of the *ab initio* enthalpy difference between fcc and bcc W. Figure 3(b) shows that significant discrepancies exist between the *ab initio*  $\Delta H_m^{\text{fcc}}$  and the values extracted independently from the phase diagram.

A set of related  $A_W$  and  $B_W$ , calculated in the way just described, is summarized in Fig. 4. An essentially linear relation is obtained, suggesting that a further increase in  $B_W$  would bring the thermodynamic predictions based on the phase diagram into good agreement with *ab initio* fcc-bcc enthalpy difference for W. This idea was tested in a fitting procedure, where all *ab initio*  $\Delta H_m^{\text{fcc}}$  values were included together with the phase diagram data, while both  $A_W$  and  $B_W$  were treated as free parameters. Then we obtained  $A_W = 32.6$  mRy/atom, and accounted approximately for  $\Delta H_m^{\text{fcc}}(x_W)$  in the whole composition range. However, the entropy difference  $B_W = 1.42R$  was large enough to make fcc W more stable than bcc W at high temperatures. This contradicts the experimental fact that bcc is the only stable form of W up to the melting point.<sup>11</sup>

We conclude that the subregular-solution analysis of the Pt-W phase diagram leads to enthalpy-of-formation values which approach (but still do not reach) the *ab initio* results only if one accepts a large entropy difference between fcc and bcc W.

#### IV. CONSEQUENCES OF A DYNAMICALLY UNSTABLE fcc W

##### A. Possible dynamical stabilization of fcc W at high temperatures

The *ab initio* results of Sec. II C show that fcc W is dynamically unstable at  $T = 0$  K against all long-

wavelength shear deformations. If such an instability remains for fcc W at all temperatures, there will be a concentration range in the Pt-W system where the vibrational entropy, and hence also the Gibbs energy, of the fcc phase is undefined. However, there is also a possibility that the lattice becomes dynamically stable at high temperatures, so that the thermodynamic functions are well defined. Such a case is exemplified by, e.g., bcc Zr which is known to be dynamically unstable at low temperatures,<sup>40</sup> but it also is the observed equilibrium phase between 1139 K and its melting point 2128 K.<sup>41</sup> If fcc W shows an analogous behavior, it results in an entropy that has a strong and unusual temperature dependence.<sup>42</sup> Also the enthalpy has a strong and anomalous temperature dependence since  $H$  and  $S$  are coupled through the heat capacity. Hence,<sup>13,14</sup> the enthalpy derived in a standard CALPHAD extrapolation for a phase that is dynamically unstable at  $T = 0$  K should not be uncritically identified with an *ab initio* value referring to 0 K, even if the phase becomes dynamically stable at high temperatures. In order to rely on phase diagram data in a prediction of the enthalpy of a metastable (and dynamically stable) phase, it is essential to have independent knowledge about the vibrational entropy.

##### B. Consequences of instability for the phase diagram

We now argue that even if fcc W is dynamically unstable at *all* temperatures, one<sup>13,43</sup> may introduce a hypothetical metastable fcc W phase that serves as an end point in the extrapolation of the Gibbs energy for fcc Pt-W alloys. This is possible because the vibrational entropy  $S_{\text{vib}}$  does not diverge as one approaches the alloy concentration of dynamical instability. Hence the Gibbs energy has a smooth behavior and can be represented by the CALPHAD ansatz. It is sufficient for our discussion to neglect anharmonic effects. The high-temperature expansion of the vibrational entropy  $S_{\text{vib}}$ , expressed in terms of the density of states  $F(\omega)$  for the phonon frequencies  $\omega$ , is<sup>24</sup>

$$S_{\text{vib}} = k_B \int_0^{\omega_{\text{max}}} \left\{ 1 + \ln \left( \frac{k_B T}{\hbar \omega} \right) + \frac{1}{24} \left( \frac{\hbar \omega}{k_B T} \right)^2 + \dots \right\} F(\omega) d\omega. \quad (16)$$

As one approaches a dynamical instability,  $F(\omega)$  increases for small  $\omega$ . However, the integral in Eq. (16) is convergent unless  $F(\omega)$  diverges as  $\omega^\alpha$ , with  $\alpha < -1$  for small  $\omega$ . Normally  $S_{\text{vib}}$  increases smoothly and tends to a finite value (see the Appendix). We have already noted the difficulty in separating the two parts of the Gibbs energy,  $H$  and  $-TS$ , using a CALPHAD fit to the phase diagram data. Suppose that we have somehow managed to obtain  $S_{\text{vib}}$ , and found that it varies significantly as a function of alloy composition. Since  $S_{\text{vib}}$  is an integrated quantity over the phonon density of states, one cannot distinguish between a dynamical instability and an overall softening of lattice vibrations from the knowledge of

$S_{\text{vib}}$  alone. It follows that the phase diagram *per se* has no feature which is accessible to CALPHAD analyses and which reveals the presence of a dynamical instability.

### C. A CALPHAD treatment of the *ab initio* results

It is essential for the thermodynamic approach to postulate the dynamical stability of a nonstable phase. Its entropy is described in the CALPHAD approach by Eq. (12). However, for reasons mentioned in Sec. IV A, this expression will not describe well the actual entropy of a high-temperature metastable phase and hence cannot be extrapolated to  $T = 0$  K. Since the thermodynamic analyses aim at the Gibbs energy of a phase,  $G = H - TS$ , an inaccurate treatment of the vibrational entropy will, generally speaking, give an enthalpy that does not correspond to the physical enthalpy. This explains why a standard CALPHAD treatment of the Pt-W phase diagram data in Sec. III C yields enthalpies of fcc  $\text{Pt}_{1-c}\text{W}_c$  which disagree with the *ab initio* results [cf. Fig. 3(b)]. Further, Fig. 3(a) shows that these calculations predict a finite solubility of Pt in bcc W at low temperatures. We consider that this prediction is an artifact of the fitting procedure due to insufficient experimental data at low temperatures.

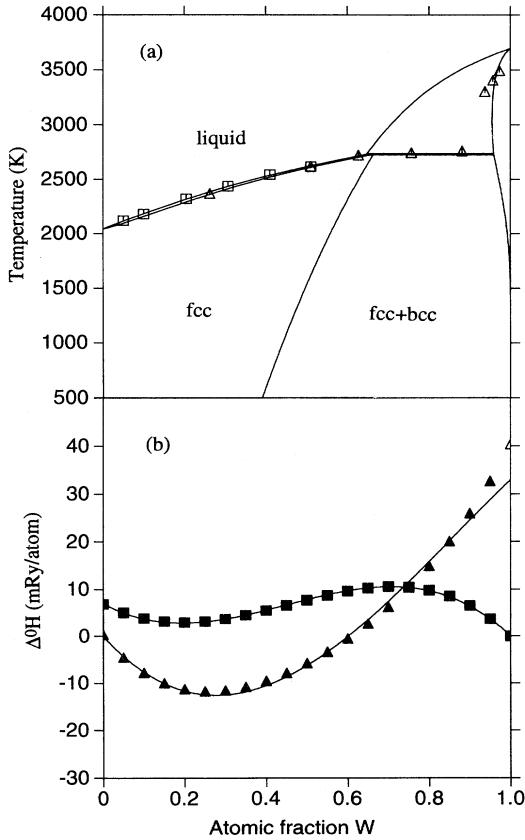


FIG. 5. As in Fig. 3, but with the *ab initio* CE values for the enthalpy of formation of bcc (squares) and fcc (triangles) solution phases included in the fit.

In an attempt to make the best use of the *ab initio* data, we include them in a CALPHAD fit, as if they were available experimental data. The excess Gibbs energy  ${}^E G_m^{\text{fcc}}$  was described by a three-term Redlich-Kister<sup>30</sup> polynomial and  ${}^E G_m^{\text{bcc}}$  was treated by using Eq. (14), but allowing  ${}^0L$  and  ${}^1L$  to vary linearly with the temperature. In addition, the possibility of a large entropy difference  $\Delta S_W^{\text{fcc/bcc}}$  was accounted for empirically by using a linear relation between  $A_W$  and  $B_W$ , as suggested by Fig. 4. *Ab initio* enthalpies of formation of fcc alloys for  $0 \leq x_W \leq 0.95$  and of bcc alloys for  $0 \leq x_W \leq 1$  were considered.

Figure 5(a) shows that the calculated Pt-W phase diagram accurately reproduces the experimental data at high temperatures. Furthermore, Fig. 5(b) demonstrates that the *ab initio* enthalpies of formation of bcc  $\text{Pt}_{1-c}\text{W}_c$  are accurately reproduced by the subregular-solution fit. The enthalpies of formation of the fcc phase agree very well for  $x_W$  up to 0.9. As expected, this calculation yields an enthalpy difference between fcc and bcc W which is lower than the *ab initio* enthalpy difference, i.e.,  $A_W = 33$  mRy/atom, and an entropy difference  $B_W = 1.396R$ ; cf. Sec. III C, where the slightly larger  $B_W = 1.42R$  was found to stabilize fcc W at high temperatures. We conclude that *ab initio* total energy data can be used successfully in a CALPHAD modeling of the Pt-W phase diagram.

### V. SUMMARY

We have performed *ab initio* electronic-structure calculations of enthalpies of formation at 0 K and vibrational properties of fcc and bcc  $\text{Pt}_{1-c}\text{W}_c$  and confronted those results with a detailed thermodynamic CALPHAD-

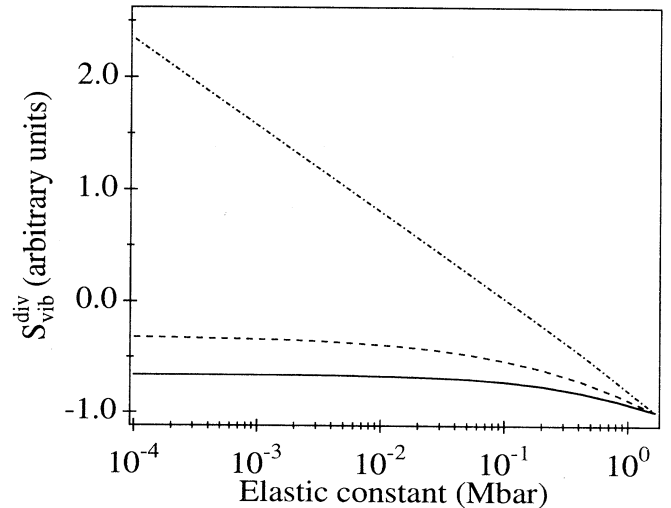


FIG. 6. The quantity  $S_{\text{vib}}^{\text{div}}$  in Eq. (A1) as a function of the elastic constants  $C'$  and  $C_{44}$ . The bulk modulus  $B = \frac{1}{3}(C_{11} + 2C_{12})$  has been set to a constant value,  $B = 3$  Mbar. The continuous line has been obtained by setting  $C_{44} = 1.65$  Mbar and varying  $C'$ , the dashed line by setting  $C' = 1.65$  Mbar and varying  $C_{44}$ , while the dash-dotted curve refers to  $C' = C_{44}$ . Note the logarithmic scale on the abscissa.

type analysis. The main objectives of the study have been the serious discrepancies between the *ab initio* and CALPHAD enthalpy differences of fcc and bcc W. We established that, contrary to some previous suggestions,<sup>4,6,31</sup> the CALPHAD approach has the mathematical flexibility to account for the variation of the enthalpy of formation as a function of composition in the fcc Pt-W system. Next we have found, in accord with some other studies,<sup>13-15</sup> that fcc W is dynamically unstable at low temperatures with respect to all long-wavelength transversal shear modes. The vibrational entropy therefore becomes very important in the W-rich side of fcc Pt-W, and we argue that it cannot be properly accounted for in a CALPHAD-type analysis. Thus we conclude, in accord with Craievich and Sanchez<sup>13</sup> and Craievich *et al.*,<sup>14</sup> that the enthalpy of metastable fcc W as deduced from a CALPHAD fit to the experimental data, should not be compared with the *ab initio* enthalpy at 0 K. However, we suggest that the CALPHAD analysis yields parameters for hypothetical metastable phases which are useful in modeling multicomponent systems. We finally note that, although lattice instabilities seem to be present for many systems with large discrepancies between CALPHAD and *ab initio* enthalpies,<sup>13,14</sup> bcc and fcc Fe provide an example where the phases are dynamically stable but the *ab initio* values of the enthalpies<sup>44,45</sup> still disagree with the thermodynamic results.<sup>1,46,47</sup>

#### ACKNOWLEDGMENTS

The authors gratefully acknowledge financial support provided by the Swedish Natural Science Research Council, The Swedish National Board for Industrial and Technical Development, The Swedish Research Council for Engineering Sciences, and the Göran Gustafsson Foundation. The work by one of us (A.F.G.) is part of a research project supported by the Consejo Nacional de Investigaciones Científicas y Técnicas of Argentina under Grant No. PIA-0028/92. Further, we gratefully acknowledge discussions with M. Hillert, L. Kaufman, A. P. Miodownik, J. M. Sanchez, and R. E. Watson.

#### APPENDIX

Consider the long-wavelength limit of lattice vibrations in a cubic crystal with elastic constants  $C_{11}$ ,  $C_{12}$ ,

and  $C_{44}$ .<sup>48</sup> When  $T \gtrsim \theta_D$ , the important contribution of a phonon mode  $(\mathbf{q}, \lambda)$  to the vibrational entropy is proportional to the logarithm of the frequency [cf. Eq. (16)], which gives for the acoustic modes  $S_{\text{vib}}(\mathbf{q}, \lambda) \propto \ln \omega(\mathbf{q}, \lambda) \propto \ln v_\lambda(\hat{q})$ .  $v_\lambda(\hat{q})$  is the sound velocity,  $\hat{q} \equiv \mathbf{q}/q$ , and  $\lambda = 1, 2, 3$  labels transverse and longitudinal branches. This contribution is divergent when  $v_\lambda(\hat{q}) \rightarrow 0$ . The total vibrational entropy due to all long-wavelength modes will depend on the following integral:

$$S_{\text{vib}}^{\text{div}} \propto \frac{1}{3} \int \ln v_1(\hat{q}) v_2(\hat{q}) v_3(\hat{q}) \frac{d\Omega_{\hat{q}}}{4\pi}. \quad (\text{A1})$$

The dependence of  $S_{\text{vib}}^{\text{div}}$ , Eq. (A1), on the two elastic constants  $C' = \frac{1}{2}(C_{11} - C_{12})$  and  $C_{44}$  is shown in Fig. 6. We see that if only one of the elastic constants tends to zero, the vibrational entropy has a finite limit. In order for the vibrational entropy to show a weak logarithmic singularity, both  $C'$  and  $C_{44}$  must tend to zero simultaneously. However, in a real and gradually changing phonon spectrum, the first modes that become unstable represent only an infinitesimal part of all phonon modes. Therefore the vibrational entropy does not diverge but has a limiting value as the critical alloy composition is approached.

We next argue that  $S_{\text{vib}}$  is convergent also in the case when the instability arises for a phonon mode of finite wave vector  $\mathbf{q}_0$ . Assuming  $\omega(\mathbf{q}_0) = 0$ , we expand the phonon frequencies near  $\mathbf{q}_0$  as

$$\begin{aligned} \omega(\mathbf{q}) &= \alpha_x (q_x - q_{0x})^2 + \alpha_y (q_y - q_{0y})^2 \\ &+ \alpha_z (q_z - q_{0z})^2. \end{aligned} \quad (\text{A2})$$

Consider the terms in  $S_{\text{vib}}$  containing  $\ln \omega(\mathbf{q})$ , in the vicinity of  $\mathbf{q}_0$ . They contribute to  $S_{\text{vib}}$  a term proportional to

$$\int \ln \left[ \alpha_x (q_x - q_{0x})^2 + \alpha_y (q_y - q_{0y})^2 + \alpha_z (q_z - q_{0z})^2 \right] d^3(\mathbf{q} - \mathbf{q}_0), \quad (\text{A3})$$

which is convergent.

<sup>1</sup> The CALPHAD method is described in L. Kaufman and H. Bernstein, *Computer Calculation of Phase Diagrams* (Academic, New York, 1970) and extensively used in contributions to CALPHAD Comput. Coupling Phase Diagrams Thermochem.

<sup>2</sup> A. P. Miodownik, in *Computer Modeling of Phase Diagrams*, edited by L. H. Bennet (The Metallurgical Society, Warrendale, 1986), p. 253.

<sup>3</sup> L. Kaufman, in *Alloy Phase Stability*, Vol. 163 of *NATO Advanced Study Institute, Series E: Applied Sciences*, edited by G. M. Stocks and A. Gonis (Kluwer Academic, Dordrecht, 1987), p. 145.

<sup>4</sup> G. Grimvall, M. Thiessen, and A. Fernández Guillermet,

Phys. Rev. **36**, 7816 (1987).

<sup>5</sup> N. Saunders, A. P. Miodownik, and A. T. Dinsdale, CALPHAD Comput. Coupling Phase Diagrams Thermochem. **12**, 351 (1988).

<sup>6</sup> A. Fernández Guillermet and M. Hillert, CALPHAD Comput. Coupling Phase Diagrams Thermochem. **12**, 337 (1988).

<sup>7</sup> M. Kosugi and J. M. Sanchez, Bull. Alloy Phase Diagrams **10**, 319 (1989).

<sup>8</sup> G. W. Fernando, R. E. Watson, M. Weinert, Y. J. Wang, and J. W. Davenport, Phys. Rev. B **41**, 11 813 (1990).

<sup>9</sup> R. E. Watson, G. W. Fernando, M. Weinert, and J. W. Davenport, J. Phase Equilibria **13**, 244 (1992).

- <sup>10</sup> A. P. Miodownik, in *Structural and Phase Stability of Alloys*, edited by J. L. Morán-López, F. Meía-Lira, and J. M. Sanchez (Plenum Press, New York, 1992), p. 65.
- <sup>11</sup> P. Gustafson, *Int. J. Thermophys.* **6**, 395 (1985).
- <sup>12</sup> D. Pettifor, quoted in Ref. 5 as a private communication.
- <sup>13</sup> P. J. Craievich and J. M. Sanchez (unpublished).
- <sup>14</sup> P. J. Craievich, M. Weinert, J. M. Sanchez, and R. E. Watson, *Phys. Rev. Lett.* **72**, 3076 (1994).
- <sup>15</sup> J. M. Wills, Olle Eriksson, Per Söderlind, and A. M. Borning, *Phys. Rev. Lett.* **68**, 2802 (1992).
- <sup>16</sup> A. Fernández Guillermét and G. Grimvall, *Phys. Rev. B* **44**, 4332 (1991).
- <sup>17</sup> J. M. Sanchez, F. Ducastelle, and D. Gratias, *Physica A* **128**, 334 (1984).
- <sup>18</sup> J. W. D. Connolly and A. R. Williams, *Phys. Rev. B* **27**, 5169 (1983).
- <sup>19</sup> Z. W. Lu, S.-H. Wei, A. Zunger, S. Frota-Pessoa, and L. G. Ferreira, *Phys. Rev. B* **44**, 512 (1991).
- <sup>20</sup> M. Methfessel, *Phys. Rev. B* **38**, 1537 (1988); M. Methfessel, C. O. Rodriguez, and O. K. Andersen, *ibid.* **40**, 2009 (1989).
- <sup>21</sup> D. M. Ceperley and B. J. Alder, *Phys. Rev. Lett.* **45**, 566 (1980).
- <sup>22</sup> S. H. Vosko, L. Wilk, and M. Nusair, *Can. J. Phys.* **58**, 1200 (1980).
- <sup>23</sup> C. Wolverton, M. Asta, H. Dreyssé, and D. de Fontaine, *Phys. Rev. B* **44**, 4914 (1991); C. Wolverton, G. Ceder, D. de Fontaine, and H. Dreyssé, *ibid.* **48**, 726 (1993).
- <sup>24</sup> G. Grimvall, *Thermophysical Properties of Materials* (North-Holland, Amsterdam, 1986).
- <sup>25</sup> M. Dacorogna, J. Ashkenazi, and M. Peter, *Phys. Rev. B* **26**, 1527 (1982).
- <sup>26</sup> K.-M. Ho, C. L. Fu, B. N. Harmon, W. Weber, and D. R. Hamann, *Phys. Rev. Lett.* **49**, 673 (1982).
- <sup>27</sup> K.-M. Ho, C. L. Fu, and B. N. Harmon, *Phys. Rev. B* **28**, 6687 (1983); **29**, 1575 (1984).
- <sup>28</sup> J. Häglund, G. Grimvall, and T. Jarlborg, *Phys. Rev.* **47**, 9279 (1993).
- <sup>29</sup> A. T. Dinsdale, *CALPHAD Comput. Coupling Phase Diagrams Thermochem.* **15**, 317 (1991).
- <sup>30</sup> O. Redlich and A. T. Kister, *Ind. Eng. Chem.* **40**, 345 (1948).
- <sup>31</sup> A. Fernández Guillermét and W. Huang, *Z. Metallkd.* **79**, 88 (1988).
- <sup>32</sup> A. Fernández Guillermét and W. Huang, *Int. J. Thermophys.* **12**, 1077 (1991).
- <sup>33</sup> A. Fernández Guillermét and S. Jonsson, *Z. Metallkd.* **84**, 106 (1993).
- <sup>34</sup> L. Müller, *Ann. Phys. (Leipzig)* **7**, 9 (1930).
- <sup>35</sup> R. Hultgren and R. I. Jaffee, *J. Appl. Phys.* **12**, 501 (1941).
- <sup>36</sup> R. Jaffe and H. P. Nielsen, *Trans. Am. Inst. Mech. Eng.* **180**, 603 (1949).
- <sup>37</sup> C. J. Smithells, *Tungsten. A Treatise on its Metallurgy, Properties and Applications* (Chapman and Hall, London, 1952), p. 271.
- <sup>38</sup> M. Hansen and K. Anderko, *The Constitution of Binary Alloys* (McGraw-Hill, New York, 1958), p. 1145.
- <sup>39</sup> A. G. Knapton, *Platinum Met. Rev.* **24**, 64 (1980).
- <sup>40</sup> Y.-Y. Ye, Y. Chen, K.-M. Ho, and B. N. Harmon, *Phys. Rev. Lett.* **58**, 1769 (1987).
- <sup>41</sup> A. Fernández Guillermét, *High Temp. High Pressures* **19**, 119 (1987).
- <sup>42</sup> In bcc Zr the instability is related to a specific point in  $\mathbf{q}$  space. However, a high-temperature stabilization of fcc W, although possible, seems unlikely because the instability occurs in an extended region in  $\mathbf{q}$  space, and, moreover, would be difficult to consider in *ab initio* calculations.
- <sup>43</sup> This approach has also been suggested by A. P. Miodownik, who introduced "effective CALPHAD values" for the metastable phase.
- <sup>44</sup> H. J. F. Jansen and S. S. Peng, *Phys. Rev. B* **37**, 2689 (1988).
- <sup>45</sup> D. J. Singh, W. E. Pickett, and H. Krakauer, *Phys. Rev. B* **43**, 11 628 (1991).
- <sup>46</sup> A. Fernández Guillermét and P. Gustafson, *High Temp. High Pressures* **16**, 591 (1985).
- <sup>47</sup> L. Kaufman, *Scand. J. Metall.* **20**, 32 (1991).
- <sup>48</sup> A. G. Every, *Phys. Rev. B* **22**, 1746 (1980).